

Training quantum machine learning models on cloud without uploading the data

Guang Ping He*

School of Physics, Sun Yat-sen University, Guangzhou 510275, China

Based on the linearity of quantum unitary operations, we propose a method that runs the parameterized quantum circuits before encoding the input data. This enables a dataset owner to train machine learning models on quantum cloud computation platforms, without the risk of leaking the information about the data. It is also capable of encoding a vast amount of data effectively at a later time using classical computations, thus saving runtime on quantum computation devices. The trained quantum machine learning models can be run completely on classical computers, meaning the dataset owner does not need to have any quantum hardware, nor even quantum simulators. Moreover, our method mitigates the encoding bottleneck by reducing the required circuit depth from $O(2^n)$ to $O(n)$, and relax the tolerance on the precision of the quantum gates for the encoding. These results demonstrate yet another advantage of quantum and quantum-inspired machine learning models over existing classical neural networks, and broaden the approaches to data security.

I. INTRODUCTION

Data security is rated more and more important nowadays. Individuals need to keep their privacy from misuse and abuse, companies want to protect their intellectual property rights, and governments are concerned about the threat to the national security. Unauthorized transfer of data may be against the law in many places. Some countries also put strict restrictions on exporting data abroad. On the other hand, the rapid development of artificial intelligence technology demands a vast amount of data as input, notably in the training of autonomous driving, intelligent healthcare systems and large language models. Meanwhile, not every data owner has very powerful computation devices at home, nor even in his own region. Especially, while quantum machine learning is generally expected to be a potential powerful tool for artificial intelligence technology, intermediate and large scale quantum computers are only available via very few cloud platforms in certain countries.

To solve the dilemma between the owner of data and the provider of computational resources, here we propose a run-before-encoding method, which can accomplish the following task. Suppose that Alice owns the dataset and Bob holds the quantum cloud computation platform. Alice can run the quantum circuits on Bob's platform beforehand, without encoding any data. Based on the output received from Bob, Alice can input her data later and calculate the cost function needed for training machine learning models on her own local classical computer. The final trained models can also be run on Alice's local classical computer. Since her data has never been sent to Bob's side, it remains perfectly secure against Bob. This merit makes the method very useful either as a standalone application or as a building block for federated learning [1–3].

This method is backed by the linearity in quantum

unitary operations, so that it is unavailable for existing classical neural networks where the activation functions of the neurons are nonlinear. Thus, it displays yet another advantage of using quantum or quantum-inspired machine learning models over existing classical counterparts.

II. TYPICAL FEATURES OF QUANTUM MACHINE LEARNING MODELS

Our method works for quantum circuits with the following features: (1) measurements are performed at the last stage only, while all the rest operations are unitary transformations, and (2) these unitary transformations need to result in real probability amplitudes only. Fortunately, a large portion of the variational quantum circuit (VQC) architecture [4–8] widely used for quantum machine learning today belongs to this category, as elaborated below.

To avoid confusion, we use $|x\rangle_2$ ($|x\rangle_{10}$) to denote the quantum states where x is understood as a binary (decimal) number. Taking the 5-qubit states as an example, we have $|0\rangle_{10} = |0\rangle_2 \otimes |0\rangle_2 \otimes |0\rangle_2 \otimes |0\rangle_2 \otimes |0\rangle_2 = |00000\rangle_2$, $|1\rangle_{10} = |00001\rangle_2$, $|2\rangle_{10} = |00010\rangle_2$, etc. Fig. 1 shows the typical architecture of a VQC, which consists of three modules: the feature map, the ansatz, and the measurement of the observables. At the beginning, the state of all the qubits on the far left are initialized as $|0\rangle_{10}$. Then the feature map serves as a unitary transformation $U_F(x)$, which actually consists of several 1-qubit and 2-qubit elementary unitary quantum gates, turning $|0\rangle_{10}$ into a certain quantum state $|x\rangle_{10}$ that encodes the input data x . There are many data-encoding methods, e.g., dense angle encoding, general qubit encoding, amplitude encoding and general amplitude encoding [9, 10]. The encoded state in all these methods can be expressed as a linear superposition of the basis vectors. That is, for an input data described by the d -dimensional feature vector $x = [x_0, \dots, x_{d-1}]^T \in R^d$, the feature map encodes it

*Electronic address: hegp@mail.sysu.edu.cn

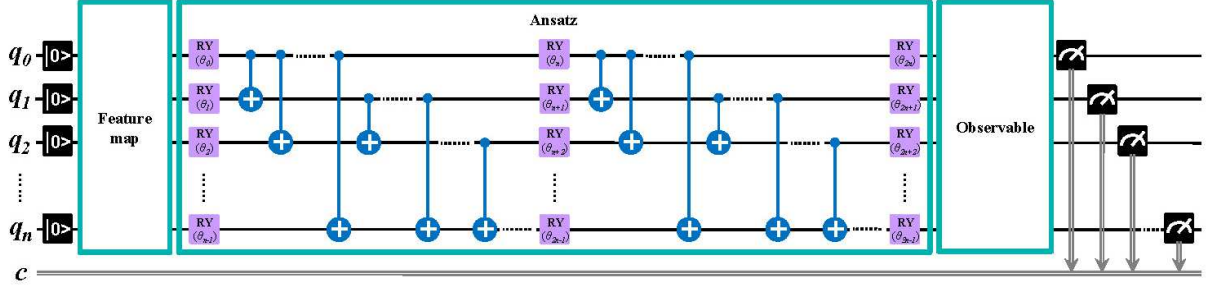


FIG. 1: A typical variational quantum circuit (VQC) with the *RealAmplitudes* ansatz. Showed with 2-repetition and full entanglement.

using the state

$$|x\rangle_{10} = U_F(x) |0\rangle_{10} = \frac{1}{C_x} \sum_{i=0}^{d-1} f_i(x) |i\rangle_{10}, \quad (1)$$

where $f_i(x)$ is a function of x , $|i\rangle_{10}$ ($i = 0, \dots, d-1$, $d \leq 2^n$) are the basis vectors of the Hilbert space of the n -qubit system, and C_x is the normalization constant.

The ansatz has many possible structures too. A widely used one is the *RealAmplitudes* ansatz [6, 8], which is the default ansatz in Qiskit's VQC implementation. It can have many repetitions and different entanglement constructions. The example in Fig. 1 is a 2-repetition one with *full entanglement* (see Sec. 1 of Supplementary Materials for explanation). The effect of the entire *RealAmplitudes* ansatz can be described by a unitary transformation $U_A(\vec{\theta})$ with $\vec{\theta}$ being a set of adjustable parameters. It has the following merit. When being applied on any n -qubit state

$$|\psi\rangle_{10} = \sum_{i=0}^{N-1} A_i |i\rangle_{10}, \quad (2)$$

if all A_i ($i = 0, \dots, N-1$, $N = 2^n$) are real numbers, then in the resultant state

$$|\psi'\rangle_{10} = U_A(\vec{\theta}) |\psi\rangle_{10} = \sum_{i=0}^{N-1} A'_i |i\rangle_{10}, \quad (3)$$

the amplitudes A'_i ($i = 0, \dots, N-1$) will remain real.

Finally, the measurement module measures a certain observable of the qubits in a certain basis. It can always be rephrased as applying a certain unitary transformation U_O on all qubits, then measuring them in the computational basis $\{|0\rangle_{10}, |1\rangle_{10}, |2\rangle_{10}, \dots, |N-1\rangle_{10}\}$. This is the only part where nonlinearity occurs in a VQC, because for each input x , the final state right before the measurement in the computational basis at the end of the VQC can be expressed as

$$|\psi_{final}(x)\rangle_{10} = \sum_{m=0}^{N-1} a_m(x) |m\rangle_{10}, \quad (4)$$

where $a_m(x)$ ($m = 0, \dots, N-1$) is the normalized probability amplitude for the basis vector $|m\rangle_{10}$. The probability for finding $|m\rangle_{10}$ is

$$p_m(x) = |a_m(x)|^2, \quad (5)$$

which is a nonlinear function.

Once $p_m(x)$ is obtained, it can be used for computing the cost function and the gradients of the adjustable parameters via classical computations [11, 12]. This completes one epoch of training.

III. OUR METHOD

Finding $p_m(x)$ is the key of the training process. In previous research, it is done simply by running the VQC using x as input. If Alice wants to use Bob's quantum cloud computation platform, she has to send x to Bob. But now we are interested in how to obtain $p_m(x)$ without sending x out of Alice's site. To this end, notice that the relationship between the initial state $|0\rangle_{10}$, the state $|x\rangle_{10}$ after applying the feature map, and the final state $|\psi_{final}(x)\rangle_{10}$ before the measurement in the computational basis is

$$|\psi_{final}(x)\rangle_{10} = U_O U_A(\vec{\theta}) U_F(x) |0\rangle_{10} = U_O U_A(\vec{\theta}) |x\rangle_{10}. \quad (6)$$

Combining with Eqs. (1) and (4), we yield

$$\sum_{m=0}^{N-1} a_m(x) |m\rangle_{10} = \sum_{i=0}^{d-1} \frac{f_i(x)}{C_x} U_O U_A(\vec{\theta}) |i\rangle_{10}. \quad (7)$$

Expanding $U_O U_A(\vec{\theta}) |i\rangle_{10}$ in the computational basis as

$$U_O U_A(\vec{\theta}) |i\rangle_{10} = \sum_{m=0}^{N-1} b_m(i) |m\rangle_{10}, \quad (8)$$

thus we have

$$a_m(x) = \sum_{i=0}^{d-1} \frac{f_i(x)}{C_x} b_m(i) \quad (9)$$

for $m = 0, \dots, N - 1$. It can be expressed in a more compact form using matrix product as

$$\vec{a}(x) = B\vec{f}(x), \quad (10)$$

where $\vec{a}(x)$ is a N -dimensional vector defined as

$$\vec{a}(x) = [a_0(x), \dots, a_m(x), \dots, a_{N-1}(x)]^T, \quad (11)$$

$\vec{f}(x)$ is a d -dimensional vector defined as

$$\vec{f}(x) = \frac{1}{C_x} [f_0(x), \dots, f_i(x), \dots, f_{d-1}(x)]^T, \quad (12)$$

and B is a $N \times d$ matrix defined as

$$B = \begin{bmatrix} b_0(0) & \cdots & b_0(i) & \cdots & b_0(d-1) \\ \vdots & \ddots & \vdots & & \vdots \\ b_m(0) & \cdots & b_m(i) & \cdots & b_m(d-1) \\ \vdots & & \vdots & \ddots & \vdots \\ b_{N-1}(0) & \cdots & b_{N-1}(i) & \cdots & b_{N-1}(d-1) \end{bmatrix}, \quad (13)$$

which is actually the first d columns of the $N \times N$ matrix representation of $U_O U_A(\vec{\theta})$.

Eqs. (8) and (10) give birth to the central idea of our method. The former implies that $b_m(i)$ ($m = 0, \dots, N - 1$) are the probability amplitudes of the state right before the final measurement of the VQC when the basis vector $|i\rangle_{10}$ ($i = 0, \dots, d - 1$) is input directly to the ansatz, skipping the feature map. Notably, $b_m(i)$ is not a function of x . Consequently, it can be calculated without transferring x from Alice to Bob. The latter equation means that Alice can try to obtain all $b_m(i)$ ($m = 0, \dots, N - 1$, $i = 0, \dots, d - 1$) (i.e., the matrix B) using Bob's quantum computation platform first. Then she can decide on the encoding method of her feature map at a later time, which determines the form of the function $f_i(x)$ and the normalization constant C_x . Finally, she substitutes the values of $b_m(i)$ received from Bob into Eq. (10) to compute $\vec{a}(x)$ and obtain all $p_m(x) = |a_m(x)|^2$ ($m = 0, \dots, N - 1$), which is simple arithmetic that can be done on her own classical computers without even using quantum simulators.

However, the probability amplitude $b_m(i)$ is not an observable. Although some quantum simulators can compute it directly, on real quantum hardware this cannot be done. Instead, real quantum computers can output the probability $p_m(|i\rangle_{10}) = |b_m(i)|^2$ only. Since $b_m(i)$ can be a complex number in general, it can be expressed as

$$b_m(i) = s_m(i) \sqrt{p_m(|i\rangle_{10})}, \quad (14)$$

where $s_m(i)$ could be any complex number of unit modulus. Fortunately, as mentioned above, the VQC studied here has the feature that the probability amplitudes $b_m(i)$ of the final state before the last measurement are always real. In this case, the possible choices are reduced

to either $s_m(i) = 1$ or $s_m(i) = -1$. Still, $p_m(|i\rangle_{10})$ alone is insufficient for determining $s_m(i)$ uniquely.

To circumvent this difficulty, we have the following trick. First, by using the basis vectors $|i\rangle_{10}$ ($i = 0, \dots, d - 1$. Note that Eq. (9) implies that $i = d, \dots, N - 1$ are not needed) as inputs to the ansatz (skipping the feature map), Alice asks Bob to compute $p_m(|i\rangle_{10})$ ($m = 0, \dots, N - 1$, $i = 0, \dots, d - 1$) on his quantum platform. Next, Bob picks one of the basis vectors as the reference state $|r\rangle_{10}$ ($r \in \{0, \dots, d - 1\}$), such that most of the output $p_m(|r\rangle_{10})$ ($m = 0, \dots, N - 1$) are nonzero. With the states $(|r\rangle_{10} + |i\rangle_{10})/\sqrt{2}$ ($i = 0, \dots, d - 1$, $i \neq r$) as inputs to the ansatz, he computes $p_m((|r\rangle_{10} + |i\rangle_{10})/\sqrt{2})$ ($m = 0, \dots, N - 1$). Then as proven in Sec. 2 of Supplementary Materials, the relative relationship between the sign of $s_m(i)$ and $s_m(r)$ can be determined as

$$s_m(i) = \begin{cases} +s_m(r), & \left(\begin{array}{l} 2p_m\left(\frac{|r\rangle_{10} + |i\rangle_{10}}{\sqrt{2}}\right) \\ > p_m(|r\rangle_{10}) + p_m(|i\rangle_{10}) \end{array} \right) \\ -s_m(r), & \left(\begin{array}{l} 2p_m\left(\frac{|r\rangle_{10} + |i\rangle_{10}}{\sqrt{2}}\right) \\ < p_m(|r\rangle_{10}) + p_m(|i\rangle_{10}) \end{array} \right) \end{cases}. \quad (15)$$

Consequently, we can write

$$s_m(i) = \sigma_m(i) s_m(r) \quad (16)$$

where $\sigma_m(i) = s_m(i)/s_m(r)$ is known. Combining with Eqs. (9) and (14), we find

$$a_m(x) = s_m(r) \sum_{i=0}^{d-1} \frac{f_i(x)}{C_x} \sigma_m(i) \sqrt{p_m(|i\rangle_{10})}. \quad (17)$$

Although $s_m(r)$ remains unknown, the fact that $(s_m(r))^2 = 1$ ensures that we are able to calculate the probability

$$p_m(x) = |a_m(x)|^2 = \left(\sum_{i=0}^{d-1} \frac{f_i(x)}{C_x} \sigma_m(i) \sqrt{p_m(|i\rangle_{10})} \right)^2. \quad (18)$$

To sum up, by using the state vectors $|i\rangle_{10}$ ($i = 0, \dots, d - 1$) and $(|r\rangle_{10} + |i\rangle_{10})/\sqrt{2}$ ($i \neq r$) as inputs (i.e., $d + (d - 1)$ states in total), which contain no information on the dataset x , Alice can compute the probabilities $p_m(|i\rangle_{10})$ and $p_m((|r\rangle_{10} + |i\rangle_{10})/\sqrt{2})$ ($m = 0, \dots, N - 1$) on Bob's quantum platform, and calculate $p_m(x)$ on her own classical computer later to complete the training of her machine learning model.

Note that if the probability $p_m(|r\rangle_{10})$ for a certain m turns out to be zero when $|r\rangle_{10}$ is chosen as the reference state, then Eq. (15) will be unable to determine the relative sign of $s_m(i)$ ($i \neq r$) because $2p_m((|r\rangle_{10} + |i\rangle_{10})/\sqrt{2}) = p_m(|r\rangle_{10}) + p_m(|i\rangle_{10})$. In this case, Bob needs to pick a second reference state $|r'\rangle_{10}$ ($r' \neq r$) such that $p_m(|r'\rangle_{10}) \neq 0$ for this specific m , and repeat the above procedure by using $(|r'\rangle_{10} + |i\rangle_{10})/\sqrt{2}$ ($i = 0, \dots, d - 1$, $i \neq r'$ and $i \neq r$) as inputs, and run

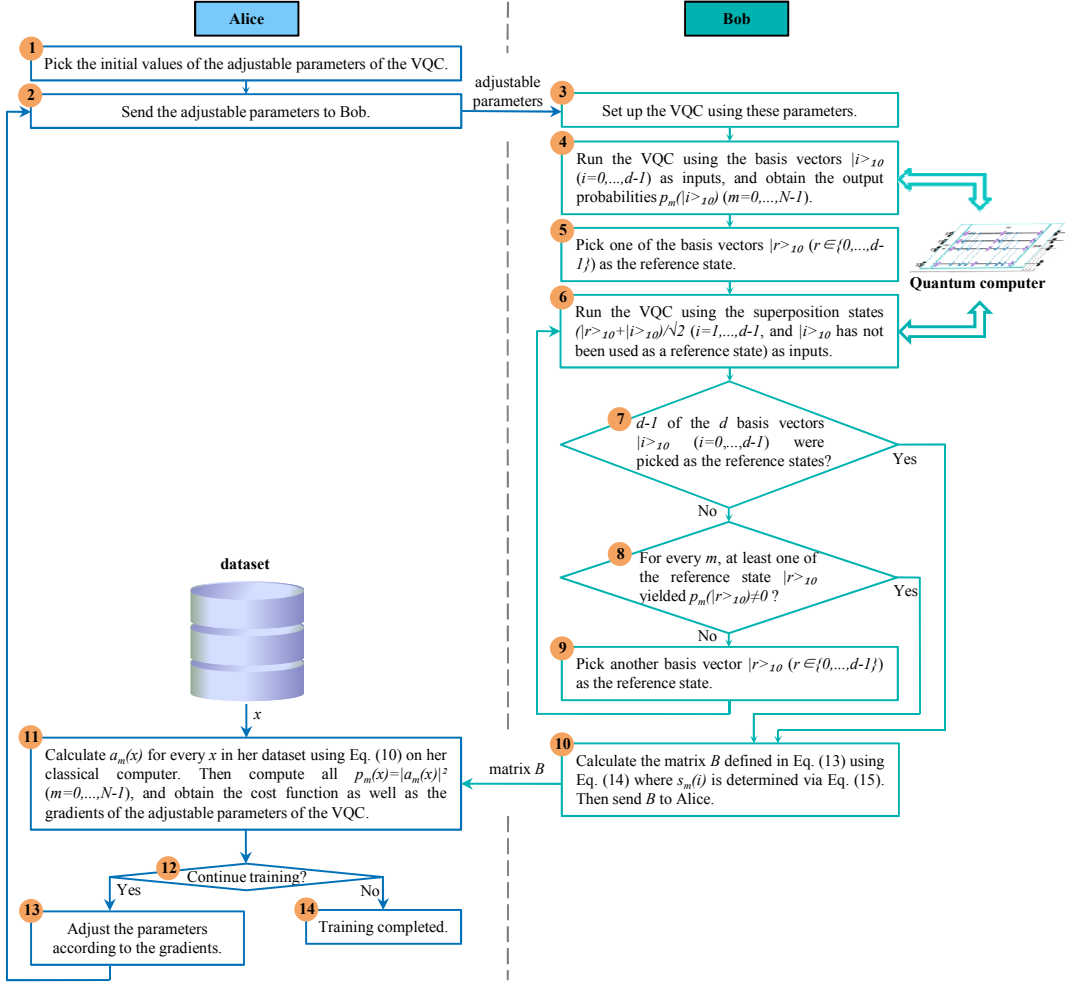


FIG. 2: Flow chart of our run-before-encoding method.

the VQC for an additional $d - 2$ times to determine $s_m(i)$. If there are still some other m for which both $p_m(|r\rangle_{10})$ and $p_m(|r'\rangle_{10})$ are zero, then he should pick a third reference state $|r''\rangle_{10}$ ($r'' \in \{0, \dots, d-1\}$, $r'' \neq r$, $r'' \neq r'$) and run the VQC using $(|r''\rangle_{10} + |i\rangle_{10})/\sqrt{2}$ ($i=1, \dots, d-1$, $i \neq r$, $i \neq r'$, $i \neq r''$) as inputs ... , until: (a) For each m , at least one of $p_m(|r\rangle_{10})$, $p_m(|r'\rangle_{10})$, $p_m(|r''\rangle_{10})$, ... is nonzero; or (b) $d-1$ of all the d basis vectors $|i\rangle_{10}$ ($i=0, \dots, d-1$) were picked as the reference states. That is, the VQC needs to be run for $d + (d-1) + (d-2) + \dots + 1 = (d+1)d/2$ times at the most. Note that in case (b), it does not matter even if there exists some certain m for which the probabilities p_m of all reference states are zero. This is because the value of $a_m(x)$ for any x will also be zero for the same m , as indicated by Eq. (9). Luckily, in our experiments to be reported below, many sets of the adjustable parameters for the VQC with randomly chosen values were tried and we always picked $|r\rangle_{10} = |0\rangle_{10}$ as the only reference state, and it turned out that all the probabilities $p_m(|r\rangle_{10})$ ($m=0, \dots, N-1$) for this $|r\rangle_{10}$ are nonzero.

Therefore, running the VQC for $d + (d-1)$ times in total is already sufficient in our experiments.

For clarity, the flow chart of the above procedure is illustrated in Fig. 2.

IV. ADVANTAGES

An obvious and foremost advantage of our method is that the security of Alice's dataset x is well-protected. As can be seen from steps (3)–(10) of the flow chart, Bob runs the VQC based on the parameters received from Alice using only the basis vectors and their superpositions as inputs. None of the data x was encoded in these states, nor being sent to Bob. In fact, the relationship between x and Bob's output may even remain unknown to Alice herself at this stage, because she does not need to decide on the encoding method and the form of the cost function until step (11). Therefore, it is clear that Bob stands no chance to learn x and the cost function.

Secondly, our method may save the runtime on quan-

tum devices when the amount of data is huge. For instance, consider the best case where all the output $p_m(|r\rangle_{10})$ ($m = 0, \dots, N - 1$) corresponding to the first reference state $|r\rangle_{10}$ are nonzero. To obtain the matrix B , the VQC needs to be run for $d + (d - 1) = 2d - 1$ input states, regardless the size of the dataset. Once B is obtained, the probability distributions corresponding to all x in the dataset can be calculated via Eq. (10) on classical computers. In contrast, when using the old method where the VQC needs to be run for each input x one by one, evaluating a dataset with s data points has to call for the VQC s times. Therefore, our method takes a much less occupancy time on quantum devices than the old one does for any dataset satisfying $s \gg 2d - 1$. As an example, the MNIST dataset [13, 14] widely used in machine learning research has a dimension $d = 784$, whereas the number of training data is $s = 50000$. In this case, our method will be significantly faster. On quantum cloud platforms charging by the runtime, less occupation of the quantum devices also means less cost.

Moreover, our method can help mitigating the encoding bottleneck [15]. In many encoding methods including the *amplitude encoding* [9], encoding a data vector x using n qubits generally requires a circuit depth of the order $O(2^n)$ [16, 17], except for certain sparse vectors. But in our method, the inputs to the VQC are merely basis vectors and simple superpositions of two basis vectors, which are indeed sparse. As proven in Sec. 3 of Supplementary Materials, in average, encoding a single basis vector takes only $n/2$ single-qubit NOT gates, while encoding the superpositions of two basis vectors takes $n/2$ single-qubit NOT gates and $n/2$ two-qubit controlled-NOT gates.

It could also relax the tolerance on the precision of the quantum gates for the encoding. For example, suppose that for an input data vector x , there is $x_i = 0.060465$, while for the same i , there is $x'_i = 0.060466$ for another input x' . When encoding using the old method, the quantum gates may need to be adjusted very precisely to show the difference. But in our method, the inputs are merely the basis vectors and their simple superpositions. Then with the same matrix B obtained from these inputs, the output of data x and x' are computed from Eq. (10) using classical arithmetic. Thus, their difference will remain visible even if the quantum gates cannot be adjusted to manifest very subtle variation.

In addition, after the training of the quantum model is completed, Alice will no longer need a quantum computer to run it. She can simply use the matrix B obtained in the final epoch of the training as the machine learning model, and applies it on any new input data x by computing Eq. (10) on her local classical computer. That is, it serves like a classical shadow model [18, 19] of the VQC. But the difference is that existing shadow models usually are merely approximations which are δ -close to the original quantum learning models, while ours works exactly as the quantum one.

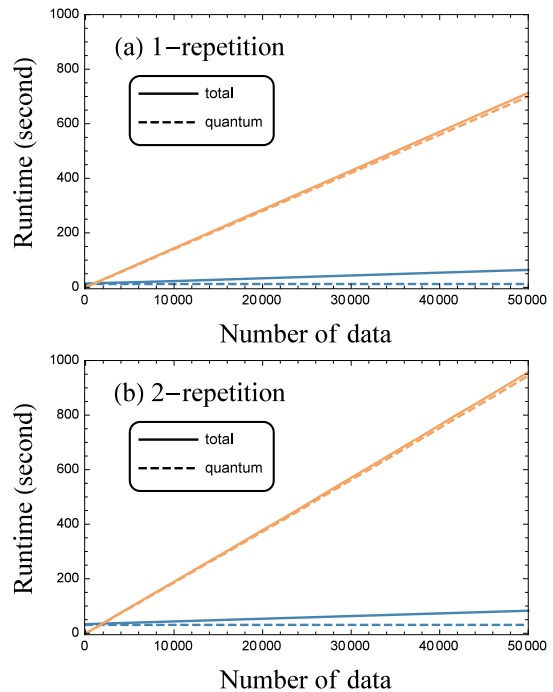


FIG. 3: Runtime of the VQC as a function of the number of input data, where the ansatz of the VQC contains (a) 1 repetition, and (b) 2 repetitions. The blues and orange lines are the results of our method and the old method, respectively. The solid lines are the time spent in total, while the dashed lines are the time spent on quantum devices.

V. EXPERIMENTAL RESULTS

We tested the runtime of our method experimentally using a 10-qubit VQC, with the training data in the MNIST dataset as inputs. Details of the VQC are provided in Sec. 1 of Supplementary Materials.

Fig. 3(a) shows the comparison between the average runtime of our model and that of the old method when the *RealAmplitudes* ansatz contains 1 repetition. (The results of the cost function turn out to be exactly the same, just as we could expect from the above equations. Therefore, it is not shown in the figure. Detailed values can be found in Data Availability section.) It is found that our method is slower when the number of data is small, but significantly faster than the old method when the number of data exceeds $d + (d - 1) = 1567$. This is because our method needs to run the VQC using the basis vectors $|i\rangle_{10}$ ($i = 0, \dots, d - 1$) and the superpositions $(|0\rangle_{10} + |i\rangle_{10})/\sqrt{2}$ ($i = 1, \dots, d - 1$) as inputs first, before computing the cost function for the first data. After this is done, the VQC is no longer needed, so that the time spent on quantum devices remains at 12.343 second unchanged, regardless the number of data, as shown by the blue dashed line. The post-processing time spent on the classical computer for calculating the cost function grows linearly as the number of data increases, resulting in a total runtime ranging from 13.682 seconds (for 1 data)

to 64.019 seconds (for 50000 data).

On the contrary, in the old method, the VQC needs to be run for every data one by one. Thus, the total runtime is only 0.102 seconds for finding the output for the first data, including 0.068 seconds spent on the quantum circuit. But then it grows linearly and is significantly slower than our method as the number of data increases. To achieve the cost function for 50000 data, the total runtime is 713.064 seconds, including 699.879 seconds spent on running the VQC.

In Fig. 3(b), the same comparison is repeated with the ansatz of VQC increased to 2 repetitions. The results show that the time spent on quantum devices running the VQC increases in both methods, while the post-processing time on the classical computer remains basically the same. Consequently, as our method needs to run the VQC for 1567 input states only, the total runtime ranges from 33.091 seconds (for 1 data) to 82.701 seconds (for 50000 data), with the time spent on quantum devices stays at 30.805 seconds regardless the number of data. On the contrary, the total runtime of the old method ranges from 0.118 seconds (for 1 data) to 957.232 seconds (for 50000 data), including the time spent on quantum devices ranging from 0.085 seconds (for 1 data) to 944.102 seconds (for 50000 data).

To sum up, these experiments verify that our method is faster than the old method when the number of data is large, and the speed-up becomes more significant with the increase of the depth of the quantum circuit. It also takes much less occupancy time on quantum devices.

VI. FURTHER IMPROVEMENTS FOR BETTER SECURITY

In our method, though Bob does not know the value of x , he knows the dimension d of x , because he is required to run the VQC for d of the basis vectors and their superpositions. He also knows the adjustable parameters of the VQC because Alice sent them to him. If these problems are the major concern while increasing the runtime on quantum devices is acceptable, we can have the following fix.

To hide the dimension of the data x , let us take the MNIST dataset as an example. Originally, Alice needs only to run the VQC for $d = 784$ basis vectors instead of all the $N = 2^{10} = 1024$ basis vectors of $n = 10$ qubits. But if Alice wants to prevent Bob from knowing that $d = 784$, she can ask Bob to run the VQC for all the 1024 basis vectors instead. Moreover, she can even ask Bob to

run a VQC with more than 10 qubits, which makes it even harder for Bob to guess the actual dimension of her data.

If Alice does not want Bob to know her choice of the adjustable parameters, she can also generate more sets of these parameters whose values are chosen differently by purpose, and ask Bob to run the VQC with these sets. This is like hiding a tree in a forest, so that Bob cannot be sure which set of the parameters is the one that Alice actually uses in her machine learning model.

VII. MORE DISCUSSION ON THE ADVANTAGE

In conclusion, we propose a run-before-encoding method so that a dataset owner Alice can train machine learning models on Bob’s quantum platform, with the primary advantage that the dataset is kept perfectly secret from Bob. Note that it was pointed out in Ref. [20] that “almost all branches of quantum machine-learning research have been heavily framed by the question of ‘beating’ classical machine learning in some figure of merit”, but “a number of ‘positive’ results have been put forward that either ‘prove’ theoretically or ‘show’ empirically that quantum computers are better at something”. But our method works for any quantum circuit where all the operations in the middle are unitary while the measurements are performed at the very end, and the unitary operations always result in real probability amplitudes. These features are not available in existing classical machine learning models but they are not uncommon for quantum ones. Thus, the advantage of our method is neither empirical nor biased towards certain tasks.

Nevertheless, this advantage can not only be achieved on real quantum computers, but also persist if Bob runs quantum simulators on classical computers. That is, though it is an advantage over all *existing* classical neural networks, strictly speaking, it may not seem appropriate to be regarded as an exclusive quantum advantage. We feel that it should be better considered as a “quantum-inspired” advantage. This result also suggests that quantum-inspired classical neural networks, i.e., redesigned classical neural networks by replacing the neuron associated by existing choices of nonlinear classical activation functions (e.g., the sigmoid, ReLU and Tanh functions) with unitary linear transformations while non-linearity occurs only at the very end, should deserve more research interests since it could make full use of the advantage in the near term.

-
- [1] Q. Yang, L. Fan, H. Yu (eds.), *Federated learning: Privacy and incentive* (Springer, Cham, 2020). Available at: <https://link.springer.com/book/10.1007/978-3-030-63076-8>.
- [2] W. Li, S. Lu, D. -L. Deng, *Sci. China Phys. Mech. As-*

- tron.* **64**, 100312 (2021). Quantum federated learning through blind quantum computing
- [3] N. Innan, M. A. -Z. Khan, A. Marchisio, M. Shafique, M. Bennai, in *2024 International Joint Conference on Neural Networks (IJCNN)* (Yokohama, Japan, 2024), pp. 1–

9. <https://doi.org/10.1109/IJCNN60899.2024.10651123>. FedQNN: Federated learning using quantum neural networks
- [4] A. Kandala, A. Mezzacapo, K. Temme, M. Takita, M. Brink, J. M. Chow, J. M. Gambetta, *Nature* **549**, 242–246 (2017). Hardware-efficient variational quantum eigensolver for small molecules and quantum magnets
- [5] M. Benedetti, E. Lloyd, S. Sack, M. Fiorentini, *Quantum Sci. Technol.* **4**(4), 043001 (2019). Parameterized quantum circuits as machine learning models.
- [6] A. Abbas, D. Sutter, C. Zoufal, A. Lucchi, A. Figalli, S. Woerner, *Nat. Comput. Sci.* **1**, 403–409 (2021). The power of quantum neural networks.
- [7] Y. Du, T. Huang, S. You, M. -H. Hsieh, D. Tao, *npj Quantum Inf.* **8**, 62 (2022). Quantum circuit architecture search for variational quantum algorithms
- [8] D. Arthur, P. Date, A hybrid quantum-classical neural network architecture for binary classification. <http://arxiv.org/abs/2201.01820> (2022).
- [9] R. LaRose, B. Coyle, *Phys. Rev. A* **102**(3), 032420 (2020). Robust data encodings for quantum classifiers.
- [10] M. Rath, H. Date, Quantum data encoding: A comparative analysis of classical-to-quantum mapping techniques and their impact on machine learning accuracy. <http://arxiv.org/abs/2311.10375> (2023).
- [11] W. Li, Z. Lu, D. -L. Deng, *SciPost Phys. Lect. Notes* **61** (2022). Quantum neural network classifiers: A tutorial.
- [12] S. Lu, L. -M. Duan, D. -L. Deng, *Phys. Rev. Research* **2**, 033212 (2020). Quantum adversarial machine learning.
- [13] Y. LeCun, *The MNIST database of handwritten digits*. <http://yann.lecun.com/exdb/mnist/> (1998).
- [14] L. Deng, *IEEE Signal Process. Mag.* **29**, 141–142 (2012). The MNIST database of handwritten digit images for machine learning research.
- [15] R. Jumade, N. Sawaya, Data is often loadable in short depth: Quantum circuits from tensor networks for finance, images, fluids, and proteins. <http://arxiv.org/abs/2309.13108> (2023).
- [16] M. Maronese, C. Destri, E. Prati, *Quantum Inf. Process.* **21**, 128 (2022). Quantum activation functions for quantum neural networks
- [17] C. -T. Li, H. -C. Cheng, Adaptive circuit learning of born machine: Towards realization of amplitude embedding and data loading. <http://arxiv.org/abs/2311.17798> (2023).
- [18] F. J. Schreiber, J. Eisert, J. J. Meyer, *Phys. Rev. Lett.* **131**(10), 100803 (2023). Classical surrogates for quantum learning models
- [19] S. Jerbi, C. Gyurik, S. C. Marshall, R. Molteni, V. Dunjko, *Nat. Commun.* **15**, 5676 (2024). Shadows of quantum machine learning
- [20] M. Schuld, N. Killoran, *PRX Quantum* **3**(3), 030101 (2022). Is quantum advantage the right goal for quantum machine learning?

Acknowledgments

This work was supported in part by Guangdong Basic and Applied Basic Research Foundation under Grant No. 2019A1515011048. The experiments were supported in part by National Supercomputer Center in Guangzhou, with the help from Qing Liu and the technical support team at National Supercomputer Center. The author also thanks Zi-Yuan Dong for valuable discussions.

Data availability

The raw experimental data of this study are publicly available at <https://github.com/gphehub/rbe2308>.

Code availability

The software codes for generating the experimental data are publicly available at <https://github.com/gphehub/rbe2308>.

Supplementary Materials

1. Experiment details

In our experiments, the feature map adopted the *amplitude encoding* method [9], i.e., a data vector $x = [x_0, \dots, x_{d-1}]^T$ is encoded as the state

$$|x\rangle_{10} = \frac{1}{C_x} \sum_{i=0}^{d-1} x_i |i\rangle_{10}. \quad (1)$$

The *RealAmplitudes* ansatz with *full entanglement* was used in our VQC. Both 1-repetition and 2-repetition were tested. Fig. 1 shows the 2-repetition architecture. It starts from a RY gate on each qubits, which introduces an independent rotation angle θ about the y -axis, turning a qubit state $\cos \gamma |0\rangle_2 + \sin \gamma |1\rangle_2$ into $\cos(\gamma + \frac{\theta}{2}) |0\rangle_2 + \sin(\gamma + \frac{\theta}{2}) |1\rangle_2$. Then several CX (controlled-NOT) gates are placed between every pairs of the qubits to make them entangled, followed by another sets of RY gates on every qubit. This completes one repetition of the *RealAmplitudes* ansatz. Adding a second repetition means adding another sets of CX gates and RY gates. The values of $\vec{\theta} = (\theta_0, \theta_1, \theta_2, \dots)$ of the RY gates are the adjustable parameters of the ansatz.

To avoid the result being biased by the status of the VQC, the adjustable parameters were chosen randomly and uniformly distributed over the interval $[0, \pi)$. With the same set of the adjustable parameters, we ran the VQC using Qiskit's quantum simulator with both our method and the old method (where each data point in the MNIST dataset is input into the VQC directly). The experiment was repeated for 10 runs, each of which used a different set of the adjustable parameters.

The form of the cost function used for each input data x is the cross entropy [11]

$$L_{CE}(\lambda) = -\frac{1}{n} \sum_{k=1}^n \lambda_k \log(g_k), \quad (2)$$

where $\lambda = (\lambda_1, \dots, \lambda_n)$ denotes the label of the input x in the form of one-hot encoding [12], g_k ($k = 1, \dots, n$) denotes the probability for the k th qubit to be found as $|1\rangle_2$ in the measurement, with $n = 10$ being the number of qubits. According to Eqs. (4) and (5) of the main text, g_k can be obtained by summing over any $p_m(x)$ where the state of the k th qubit in $|m\rangle_{10}$ is $|1\rangle_2$.

We recorded the runtime of one epoch of training as a function of the number of data being evaluated. It was found that the runtime varies only slightly in different runs, indicating that it is less affected by the values of the adjustable parameters. Therefore, we took the average of the runtime of these runs as the final result to draw Fig.3. The standard deviations were supplied in the link provided in Data Availability section, which also includes the values of all adjustable parameters and the runtime in each run.

All experiments were run on a personal laptop with a 2.8 GHz quad-core Intel i7-3840QM processor and 16 GB 1,600 MHz DDR3 memory.

2. Determining the sign of the probability amplitudes

In our method, at first when the basis vectors $|i\rangle_{10}$ ($i = 0, \dots, d-1$) are used as inputs to the ansatz, from Eqs. (8) and (14) of the main text we yield

$$U_O U_A(\vec{\theta}) |i\rangle_{10} = \sum_{m=0}^{N-1} s_m(i) \sqrt{p_m(|i\rangle_{10})} |m\rangle_{10}. \quad (3)$$

Secondly, when the states $(|r\rangle_{10} + |i\rangle_{10})/\sqrt{2}$ ($i = 0, \dots, d-1$, $i \neq r$) are used as inputs, similar to the above equation, now we have

$$U_O U_A(\vec{\theta}) \left(\frac{|r\rangle_{10} + |i\rangle_{10}}{\sqrt{2}} \right) = \sum_{m=0}^{N-1} \left(s_m \left(\frac{|r\rangle_{10} + |i\rangle_{10}}{\sqrt{2}} \right) \sqrt{p_m \left(\frac{|r\rangle_{10} + |i\rangle_{10}}{\sqrt{2}} \right)} \right) |m\rangle_{10}. \quad (4)$$

Due to the linearity of the unitary transformation $U_O U_A(\vec{\theta})$, the left-hand side of this equation can be expressed using the above Eq. (3) as

$$\begin{aligned} & U_O U_A(\vec{\theta}) \left(\frac{|r\rangle_{10} + |i\rangle_{10}}{\sqrt{2}} \right) \\ &= \frac{1}{\sqrt{2}} (U_O U_A(\vec{\theta}) |r\rangle_{10} + U_O U_A(\vec{\theta}) |i\rangle_{10}) \\ &= \sum_{m=0}^{N-1} \frac{1}{\sqrt{2}} (s_m(r) \sqrt{p_m(|r\rangle_{10})} + s_m(i) \sqrt{p_m(|i\rangle_{10})}) |m\rangle_{10}. \end{aligned} \quad (5)$$

Comparing with the right-hand side of Eq. (4), we find

$$\begin{aligned} & \frac{1}{\sqrt{2}} \left(s_m(r) \sqrt{p_m(|r\rangle_{10})} + s_m(i) \sqrt{p_m(|i\rangle_{10})} \right) \\ &= s_m \left(\frac{|r\rangle_{10} + |i\rangle_{10}}{\sqrt{2}} \right) \sqrt{p_m \left(\frac{|r\rangle_{10} + |i\rangle_{10}}{\sqrt{2}} \right)}. \end{aligned} \quad (6)$$

Recall that $s_m(i) = \pm 1$ which gives $(s_m(i))^2 = 1$ and $1/s_m(i) = s_m(i)$ (so do $s_m(r)$ and $s_m((|r\rangle_{10} + |i\rangle_{10})/\sqrt{2})$), there is

$$\begin{aligned} & \left(\frac{1}{\sqrt{2}} \left(s_m(r) \sqrt{p_m(|r\rangle_{10})} + s_m(i) \sqrt{p_m(|i\rangle_{10})} \right) \right)^2 \\ &= p_m \left(\frac{|r\rangle_{10} + |i\rangle_{10}}{\sqrt{2}} \right). \end{aligned} \quad (7)$$

Therefore

$$s_m(i) = \frac{1}{2\sqrt{p_m(|r\rangle_{10})p_m(|i\rangle_{10})}} \left(2p_m \left(\frac{|r\rangle_{10} + |i\rangle_{10}}{\sqrt{2}} \right) - (p_m(|r\rangle_{10}) + p_m(|i\rangle_{10})) \right) \cdot s_m(r). \quad (8)$$

Since $\sqrt{p_m(|r\rangle_{10})p_m(|i\rangle_{10})} > 0$, we arrive at

$$s_m(i) = \begin{cases} +s_m(r), & \left(\begin{array}{l} 2p_m \left(\frac{|r\rangle_{10} + |i\rangle_{10}}{\sqrt{2}} \right) \\ > p_m(|r\rangle_{10}) + p_m(|i\rangle_{10}) \end{array} \right) \\ -s_m(r), & \left(\begin{array}{l} 2p_m \left(\frac{|r\rangle_{10} + |i\rangle_{10}}{\sqrt{2}} \right) \\ < p_m(|r\rangle_{10}) + p_m(|i\rangle_{10}) \end{array} \right). \end{cases} \quad (9)$$

Thus, Eq. (15) in Sec. III is proven.

3. Number of quantum gates needed for encoding the input vectors of our method

Here we prove that encoding the basis vectors and the simple superposition states $(|r\rangle_{10} + |i\rangle_{10})/\sqrt{2}$ takes $O(n)$ quantum gates in average only, thus mitigating the encoding bottleneck.

(1) Encoding the basis vectors:

Any basis vector of a n -qubit system can be written as $|b_1 b_2 \dots b_n\rangle_2 = |b_1\rangle_2 |b_2\rangle_2 \dots |b_n\rangle_2$ where $b_j \in \{0, 1\}$ ($j = 1, 2, \dots, n$). To prepare such a vector from the initial state $|0\rangle_2 |0\rangle_2 \dots |0\rangle_2$ of the quantum circuit, all we need is to turn the j th qubit from $|0\rangle_2$ to $|1\rangle_2$ for any j that satisfies $b_j = 1$. This can be done by simply putting a single-qubit NOT gate on the j th qubit. For example, to prepare $|00\dots 011\rangle_2$, we need to put two NOT gates on the last two qubits. To prepare $|11\dots 111\rangle_2$, we need n NOT gates in total. Therefore, in average, encoding a single basis vector needs $n/2$ NOT gates.

(2) Encoding the superpositions of two basis vectors:

In this case, we want to achieve the state $(|r\rangle_{10} + |i\rangle_{10})/\sqrt{2} = (|r_1 r_2 \dots r_n\rangle_2 + |i_1 i_2 \dots i_n\rangle_2)/\sqrt{2}$ where $r_j, i_j \in \{0, 1\}$ ($j = 1, 2, \dots, n$). Since $i \neq r$, there exists at least one j_0 such that $r_{j_0} \neq i_{j_0}$. Without loss of generality, we can further assume that $r_{j_0} = 0$ and $i_{j_0} = 1$ (if $r_{j_0} = 1$ and $i_{j_0} = 0$, then the state can be rewritten as $(|i\rangle_{10} + |r\rangle_{10})/\sqrt{2}$ so that this assumption still holds).

Therefore, we can first prepare the state $|r_1 r_2 \dots r_n\rangle_2$ from the initial state $|0\rangle_2 |0\rangle_2 \dots |0\rangle_2$, which takes $n/2$ single-qubit NOT gates in average. Then we put a single-qubit Hadamard gate on the j_0 th qubit, turning its state into $(|0\rangle_2 + |1\rangle_2)/\sqrt{2}$. Finally, for any j that satisfies $r_j \neq i_j$ ($j \neq j_0$), we put a two-qubit controlled-NOT gates with the j_0 th qubit as the control qubit and the j th qubit as the target qubit and the job is done. This generally takes $n/2$ two-qubit controlled-NOT gates in average, because when taking all possible values of $r_1 r_2 \dots r_n$ and $i_1 i_2 \dots i_n$ into consideration, the probability for finding $r_j \neq i_j$ is $1/2$. For example, to achieve $(|0000\rangle_2 + |0110\rangle_2)/\sqrt{2}$, what we needs is to put a Hadamard gate on the 2nd qubit of the initial state $|0000\rangle_2$ so that it becomes $(|0000\rangle_2 + |0100\rangle_2)/\sqrt{2}$. Then a controlled-NOT gates with the 2nd qubit as the control qubit and the 3rd qubit as the target qubit will complete the encoding. Or suppose that we want to achieve $(|0111\rangle_2 + |1000\rangle_2)/\sqrt{2}$. The first step is to put three single-qubit NOT gates on the 2nd, 3rd and 4th qubits of the initial state $|0000\rangle_2$, respectively, so that it becomes $|0111\rangle_2$. Then a Hadamard gate on the 1st qubit turns the state into $(|0111\rangle_2 + |1111\rangle_2)/\sqrt{2}$. Now taking the 1st qubit as the control qubit, with three two-qubit controlled-NOT gates where the target qubit are taken as the 2nd, 3rd and 4th qubits, respectively, we eventually arrive at the state $(|0111\rangle_2 + |1000\rangle_2)/\sqrt{2}$.

Actually, in the above process, if we need to put a single-qubit NOT gate on a specific qubit when turning the initial state $|0\rangle_2 |0\rangle_2 \dots |0\rangle_2$ into $|r_1 r_2 \dots r_n\rangle_2$, and further turning it into the final state happens to take another two-qubit controlled-NOT gate with the same qubit as the target qubit (which occurs with probability $1/2$), then these two gates can be merged into a single two-qubit negative controlled-NOT gate (a.k.a. anti-CNOT gate, which keeps the target qubit unchanged when the state of control qubit is $|1\rangle_2$, and applies the NOT operation on the target qubit when the state of control qubit is $|0\rangle_2$). If this gate is available as an elementary gate in the quantum hardware, then encoding the above superpositions of two basis vectors needs only $n/4$ single-qubit NOT gates and $n/2$ two-qubit gates (including both the controlled-NOT and negative controlled-NOT gates) in average.